Diffusion of Hydrogen on and through γ-Iron by Density Functional Theory

Urslaan K. Chohan [a,*], *Sven P. K. Koehler*[b,c], *Enrique Jimenez-Melero*[a]

[a]School of Materials, The University of Manchester, Manchester M13 9PL, UK

[b]School of Science and the Environment, Manchester Metropolitan University, Manchester M1 5GD, UK

[c]Photon Science Institute, The University of Manchester, Manchester M13 9PL, UK

*Corresponding author.

Email: urslaan.chohan@postgrad.manchester.ac.uk

University of Manchester

School of Materials

Oxford Road

Manchester

M13 9PL

United Kingdom

Abstract

This study is concerned with the early stages of hydrogen embrittlement on an atomistic scale. We employed density functional theory to investigate hydrogen diffusion through the (100), (110) and (111) surfaces of γ-Fe. The preferred adsorption sites and respective energies for hydrogen adsorption were established for each plane, as well as a minimum energy pathway for diffusion. The H atoms adsorb on the (100), (110) and (111) surfaces with energies of ~4.06, ~3.92 and ~4.05 eV, respectively. The barriers for bulk-like diffusion for the (100), (110) and (111) surfaces are ~0.6, ~0.5 and ~0.7 eV, respectively. We compared these calculated barriers with previously obtained experimental data in an Arrhenius plot, which indicates reasonable agreement between experimentally measured and theoretically predicted activation energies. Texturing austenitic steels such that the (111) surfaces of grains are preferentially exposed at the cleavage planes may be a possibility to reduce hydrogen embrittlement.

Keywords: gamma iron, hydrogen embrittlement, hydrogen diffusion, potential energy surface, surface relaxation, density functional theory

1. Introduction

Hydrogen embrittlement (HE) is a process critical to the degradation of materials as it affects the integrity of a range of structural materials such as steels [1, 2] and nickel-based alloys [3, 4]. The HE process can lead to premature failure in those structures, which can have catastrophic consequences across a range of practical applications such as in the nuclear industry and steel oil/gas pipelines. The cost of material failure can be significant, such as the failure of steel bolts due to HE in a single high-rise office block, costing over £6M [5]. In the HE process, hydrogen enters the bulk structure of metals via diffusion, which leads to the gradual accumulation of hydrogen and a resulting increase in the brittleness of the material. There are two main mechanisms proposed for the HE phenomenon, namely the HELP (hydrogen enhanced localised plasticity) and HEDE (hydrogen enhanced decohesion) mechanisms. In HELP, hydrogen lowers the activation energy for dislocation motion, which allows the rapid initiation and propagation of a crack tip and thus enhances plastic deformation [6, 7]. In HEDE, the hydrogen favours the cleavage of planes along grain boundaries [8, 9].

Prior to hydrogen atoms entering the bulk structure, the atoms typically adsorb at specific lowest energy sites above the surface. They can subsequently diffuse into the bulk, and are likely to travel on or close to the minimum energy path (MEP), depending on the available energy. However, since a complete mechanistic understanding of the entire HE process has not yet been developed [10], we attempted to calculate this MEP to shed more light on the diffusion process in austenitic steels.

In this research project, we investigate the hydrogen adsorption and sub-surface diffusion through the (100), (110) and (111) surfaces of the face-centred cubic (fcc) phase of γ-Fe. This phase is the base in austenitic steels used in e.g. nuclear reactor applications, in the pipelines of reactors [11], and also (ultra-)high strength steels for the automotive industry [12,

13]. At above 1000 K, the γ phase crystallises [14], or at lower temperatures using γ-stabilising alloying elements such as manganese, nickel or carbon [15]. Most of the previous work focuses on hydrogen diffusion through bulk γ-Fe and along defects such as dislocation lines [16], stacking faults [17] and grain boundaries [18]. Also, the majority of the past studies concerned with hydrogen diffusion on and through iron focus on the body-centred cubic α-phase [19, 20].

Density functional theory (DFT) has previously been shown to efficiently model diffusion of hydrogen [21], which is a critical step in the HE process [22]; therefore, we have chosen to apply DFT to model hydrogen diffusion in γ-Fe to elucidate the early stages of HE in this phase relevant to austenitic steels. The investigation of the potential energy surface (PES) that governs diffusion provides critical insight into the energetics of the process and affords a detailed understanding of the on-surface adsorption and diffusion process through γ-Fe.

A PES is a multidimensional map of the energy of a chemical system as a function of the degrees of freedom in that system. Higher-dimensional PESs become increasingly difficult to represent graphically. However, an insight into any process can be derived by limiting the degrees of freedom that are considered. In the diffusion process treated here, this entails tracing the energy of a hydrogen atom diffusing through a metallic slab as a function of the x and y coordinates, as well as the depth within the slab, i.e. below the surface. To calculate the PES for the present process, the energy of a single H atom is calculated at a number of points on a regularly-spaced 3D grid of our metal slab, beginning with a plane above the surface, and inwards towards the bulk. At each depth, a 2D (reduced-dimensionality) PES produced, which yields the minimum energy site towards which the hydrogen atom would preferentially move within that plane. Above the surface, the 2D map yields the preferential site for H atom adsorption. Connecting each minimum energy point along the slab for each 2D map approximates a MEP for H diffusion from the surface into the bulk.

2. Computational Method

The potential energy surfaces for hydrogen diffusion on the surface and into sub-surfaces of γ-Fe were calculated for the (100), (110) and (111) surfaces, using density functional theory (DFT). All calculations were conducted using the Vienna *ab initio* simulation package (VASP) [23], which uses a plane-wave basis set and 3D periodic boundary conditions to describe electronic interactions. The exchange and correlation effects were included using the generalised-gradient approximation (GGA), via the Perdew-Burke-Erzenhof (PBE) functional [24]. The projector augmented-wave (PAW) approximation describes the interaction between the ionic core and valence electrons [25].

A seven layer slab model was used to model surfaces and bulk of γ-Fe. The lattice parameter, a, for γ-Fe was calculated to be 3.43 Å, with $c/a = 1$, which is in reasonable agreement with previous calculations (3.45 Å [26-28], 3.49 Å [29]) and the experimental value of 3.56 Å [30]. A (2×2) cell was applied in all calculations. A cutoff energy of 400 eV and a vacuum spacing of 20 Å were found to sufficiently converge the total energy of the system. The Methfessel Paxton method of order $N = 1$ with width 0.1 eV was used to apply electronic smearing [31]. The slabs were minimised using the conjugate gradient method [32], until forces were within 10^{-5} eV/Å. The three bottom layers were ionically constrained. The energies of all atoms were converged to within 10^{-6} eV.

The Monkhorst-Pack algorithm [33] was used with a grid size of 7×7×1 for the (100), (110) and (111) surfaces.

A mesh grid was used to sample various hydrogen positions within the slab. A large number of points was used to create a tight mesh, which would accurately describe the potential energy surface. The mesh constituted of a 6×6 uniform grid in the x-y plane, sampling only a quarter of the surface unit cell due to symmetry considerations, i.e. sampling on the domain $x,y \in$

[0,0.5], in fractional coordinates; however, this domain was expanded by appropriate mirroring to yield 144 point on the surface unit cell. This mesh was then repeated along the *z* direction of the slab (i.e. into the bulk) in uniform intervals at 9 depth; there are four 2D meshes at the first four Fe layers, there are four further 2D meshes centrally in between these Fe layers, and finally one mesh above the surface to simulate adsorption. The mesh is illustrated in

Figure **1** for each surface. For each point of the mesh, a single H atom was placed, with all coordinates constrained, and the energy of the slab was minimised by allowing all Fe atoms in the first four layers to relax. The energies at each point, *E*, were calculated via the relation

$$E = E_{\mathrm{slab+H}} - (E_{\mathrm{slab}} + E_{\mathrm{H}}) \quad (1)$$

where $E_{\mathrm{slab+H}}$ is the energy of the slab with H incorporated, E_{slab} is the energy of the H-free slab and E_{H} is the ground state energy of a single free H atom in a 10 × 10 × 10 Å^3 box. The energies were then calculated relative to the global minimum of the entire slab, which was set to 0 eV.

3. Results and Discussion

3.1 Surface adsorption on Fe (100), (110) and (111) surfaces

The adsorption of hydrogen on the (100), (110) and (111) surfaces of γ-Fe was investigated to find the preferred site of adsorption. A 6 × 6 mesh grid was placed above each surface and the energy was minimised at each point. The adsorption energy was then calculated via Eq. 1. The results are illustrated in Table 1. For the (100) surface, it was found that the H prefers to reside at the fourfold hollow (4f) site, where the Fe atoms are equidistant to one another, with an adsorption energy of 4.06 eV per H atom relative to a free H atom. For the (110) surface, the H atom prefers to reside at the short-bridge (sb) site, which is the shortest distance between two Fe atoms, with an adsorption energy of 3.92 eV per H atom. On the (111) surface, the H atom prefers to adsorb on the three-fold (3f) site, which, similar to the (100) surface, is the point where the Fe atoms are equidistant from one another; the corresponding adsorption

energy is 4.05 eV per H atom. Thus, H atoms bind most tightly to the (100) surface, however the energies are very close to one another between all three surfaces, with a mere 0.01 eV difference between the (100) and (111) surfaces. This negligible difference is within the error of our method. More importantly, for a polycrystalline sample of γ-Fe, this means that H is almost equally likely to adsorb no matter which surface is exposed, i.e. the initial step of HE, the adsorption of H to the surface, is almost independent of the crystalline structure of γ-Fe.

3.2 Subsurface diffusion of hydrogen through gamma-Fe surfaces

The process of diffusion from the surface to the sub-surfaces was modelled by investigating the potential energy surface of the whole slab. A series of calculations was conducted by creating a 2D 6×6 mesh grid at nine uniformly spaced points along the depth of the slab, starting from above the surface through to the fourth layer. Hydrogen was placed at each of those 324 points and the energy of the slab minimised by letting the Fe atoms relax in all three dimensions. For each of the (100), (110) and (111) surfaces, the MEP for diffusion was found by connecting the (energy) minima at each of the nine sampled depths. A reduced cell was considered for sampling, as illustrated in Figs. 2(c), 3(c) and 4(c), because of symmetry considerations. Important subsurface sites such as the octahedral and tetrahedral sites were sampled using the mesh method for each surface.

For all three surfaces considered, it was found that a potential barrier needs to be overcome in order for the hydrogen to penetrate the γ-Fe slab. This barrier is ~1.4 eV for the (100) surface, ~1.2 eV for the (110) surface and ~1.7 eV for the (111) surface, see Figures 2(b), 3(b), and 4(b). Therefore, most energy is required to drive the hydrogen into the (111) surface; this has deeper implications, namely that a first consideration for preventing HE would be to consider producing a textured material, such that the most exposed surface is the (111) plane parallel to the surface of the material.

The H trajectory for diffusion perpendicular to the three surfaces does not follow a linear path into the bulk, but instead the hydrogen diffuses to trapping sites along the way, moving between local maxima and minima along this pathway, see Figures 2, 3, and 4, (b) and (c), respectively. For the (100) surface, we found that the local hydrogen minima are located in the plane of Fe atoms for all sub-surfaces, and these local minima are located at the octahedral sites. The energetics of this process indicate that near the surface, there is a distinct trajectory that is traversed by the hydrogen atom, as compared to the trajectory of the H atom in the region closer to the bulk layers. Similarly, for the (110) surface, there are local minima in each of the sub-surface planes containing Fe atoms; these local minima are at the high-symmetry sites, namely alternatively the long and short-bridge sites. Due to the non-orthogonal unit cell structure for the (111) surface, and the ABCABC packing structure, the trajectory and respective energetics for the (111) surface is most complex. In contrast to the (100) and (110) surfaces, however, we observe the local minima for the H atoms to be in-between the planes containing Fe atoms, and the local maxima in the planes containing Fe atoms.

We have hence calculated the MEP of hydrogen atoms moving from the surface into the bulk, and can estimate from the local minima and maxima the barriers for absorption of the H from the surface into the bulk, and the barriers for diffusion from one sub-surface layer to the next. The activation energies, E_a, obtained can then be compared to experimentally measured diffusion energies from previous investigations. The Arrhenius equation relates the reaction rate – or in this case the diffusion coefficient of hydrogen atoms, D - to the temperature T

$$D = D_0 \exp\left(-\frac{E_a}{kT}\right) \tag{3}$$

where D_0 is the diffusion coefficient at infinite temperature (in $m^2\,s^{-1}$), and k is the Boltzmann constant (in eV K^{-1}). Hence plotting ln D against $1/T$ allows a quantitative comparison of the experimental data from literature, as shown in Fig. 5. We compared the activation energies

obtained in our calculations with those measured in austenitic stainless steels; these typically contain alloying elements, of course, while we investigated pure γ-Fe. However, our simulation box contained 28 Fe atoms only, but we only followed the MEP through the first ten Fe atoms, hence a 10% alloy would only replace one Fe atom on average, and we hereby make the assumption that low-concentration alloying elements would only have a small effect on the overall energetics of diffusion; however, we stress that this is an approximation only. It was found that in the experiments, using a range of techniques such as thermal desorption and hydrogen permeation testing, E_a was ~0.5 – 0.7 eV [34-42]. In our investigation, we calculated two activation energies, namely the total activation energy and the bulk-like activation energy for diffusion. The total activation energies were ~1.4 eV for the (100) surface, ~1.2 eV for the (110) surface and ~1.7 eV for the (111) surface, whilst the bulk-like activation energies were ~0.6, 0.5 and 0.7 eV for the (100), (110) and (111) surfaces, respectively. Whilst the total energy barrier is approximately twice the barrier as measured in the experiments, the bulk-like activation energy fits the experimental values closely. These activation energies indicate that it takes a large amount of energy to initially embed the hydrogen into each given surface, whilst it takes relatively lower amounts of energy to then continue the diffusion in the bulk element. The experiments measured the energies for the diffusion of hydrogen in the bulk, lending to the understanding that our bulk energies. It is worth noting that the activation energies for all three surfaces are quite close in the bulk-like region, with the (110) surface having the lowest activation energy. Thus the hydrogen may have a particular preference for passing through the (110) surface whilst diffusing in a polycrystalline system, it is possible that the hydrogen may also penetrate via the other surfaces. However, a larger total barrier must be overcome for the hydrogen to penetrate through the other surfaces.

The overall agreement between our values and experimental values shows our methodology produces a reasonable approximation of the barrier of diffusion, and delivers a diffusion

trajectory through bulk Fe. While adsorption to the three different surfaces considered is energetically similar, the barrier for diffusion is highest for the (111) surface, such that diffusion could be limited even in a polycrystalline sample of a textured surface were produced which preferentially exposes grains with the (111) surface to the hydrogen source.

4. Conclusions

In this study, we applied density functional theory to investigate hydrogen diffusion through the three major planes in γ-Fe, namely the (100), (110) and (111) surfaces. This study is relevant for an understanding of the most critical stages of hydrogen embrittlement, namely the adsorption and diffusion stages. The adsorption sites for H on the surface were found for each given plane, along with the adsorption energy. A minimum energy pathway for diffusion was approximated by conducting a series of energy minimisations, where H atoms were placed in a 6×6 mesh and at nine depths along the slab, starting from above the surface and including the fourth layer. It was found that for the (100) surface, the H atom preferentially adsorbs at the fourfold site, with an adsorption energy of ~4.06 eV. On the (110) surface, the H atom prefers to adsorb at the short-bridge site, with an adsorption energy of ~3.92 eV. Finally, on the (111) surface, the H atom prefers to reside at the threefold site, with an adsorption energy of ~4.05 eV. Thus, the H atom is most tightly bound to the (100) and the (111) surface. For the (100) surface, there is a ~0.6 eV barrier for bulk-like diffusion into the sub-surfaces, whilst for the (110) surface there is a ~0.5 eV barrier for bulk-like diffusion into the sub-surfaces. For the (111) surface, there is a barrier of ~0.7 eV. These barriers are in reasonable agreement with experimental data, which is shown via Arrhenius plots comparing our calculated and previous experimental data. It appears that one way to reduce hydrogen embrittlement in γ-Fe would be to produce textured austenitic materials with the (111) surface exposed.

Acknowledgements

We would like to thank the Engineering and Physical Sciences Research Council UK (EPSRC) through the Centre for Doctoral Training in Advanced Metallic Systems for the financial support (EP/L016273/1). We gratefully acknowledge the Dalton Cumbrian Facility, partly funded by the Nuclear Decommissioning Authority (NDA), for providing funding to cover the cost of computational time.

References

[1] Frohmberg, R. P., Barnett, W. J. and Troiano, A. R. (1954) *Delayed failure and hydrogen embrittlement in steel*, CASE Inst. of Tech. Cleveland OH.

[2] Moroz, L. S. and Mingin, T. E. (1962) Hydrogen embrittlement of steel. *Met. Sci. Heat Treat.* **4**(3) 135-137.

[3] Lynch, S. P. (1979) Hydrogen embrittlement and liquid-metal embrittlement in nickel single crystals. *Scr. Metall.* **13**(11) 1051-1056.

[4] Lassila, D. and Birnbaum, H. K. (1984) *Hydrogen Embrittlement of Nickel*, Illinois Univ. at Urbana Dept. of Metallurgy and Mining Engineering.

[5] Jothi, S., Sebald, T., Davies, H. M., Reese, E. D. and Brown, S. G. R. (2016) Localized microstructural characterization of a dissimilar metal electron beam weld joint from an aerospace component. *Mater. Desi.* **90** 101-114.

[6] Birnbaum, H. K. and Sofronis, P. (1994) Hydrogen-enhanced localized plasticity - a mechanism for hydrogen-related fracture. *Mater. Sci. Eng. A* 191-202.

[7] Abraham, D. P., Altstetter, C.J. (1995) Hydrogen-enhanced localization of plasticity in an austenitic stainless steel. Metallurgical and Materials transactions A.

[8] Troiano, A. R. (1960) The role of hydrogen and other interstitials on the mechanical behavior of metals. *Trans. Am. Soc. Met.*

[9] Oriani, R. A. (1978) Hydrogen embrittlement of steels. *Annu. Rev. Mat. Sci.* . **8**(1) 327-357.

[10] Strudel, J. L., Cahn, R. W. and Haasen, P. (1983) Physical Metallurgy. 1412-1481.

[11] Anoop, M. B., Rao, K. B. and Lakshmanan, N. (2008) Safety assessment of austenitic steel nuclear power plant pipelines against stress corrosion cracking in the presence of hybrid uncertainties. *Int. J. Pres. Ves. Pip.* **85**(4) 238-247.

[12] Scott, C., Allain, S., Faral, M. and Guelton, N. (2006) The development of a new Fe-Mn-C austenitic steel for automotive applications. *Metall. Res. Technol.* **103**(6) 293-302.

[13] Koyama, M., Akiyama, E. and Tsuzaki, K. (2012) Hydrogen embrittlement in a Fe–Mn–C ternary twinning-induced plasticity steel. *Corros. Sci.* **54** 1-4.

[14] Anderson, O. L. (1986) Properties of iron at the Earth's core conditions. *Geophys. J. Int.* **84**(3) 561-579.

[15] Gruzin, P. L., Grigorkin, V. I. and Moskaleva, L. N. (1969) Transformations in austenitic manganese steel. *Met. Sci. Heat Treat.* **11**(1) 5-8.

[16] Tsong-Pyng, P. and Altstetter, C. J. (1986) Effects of deformation on hydrogen permeation in austenitic stainless steels. *Acta Metall.* **34**(9) 1771-1781.

[17] Juan, A., Moro, L., Brizuela, G. and Pronsato, E. (2002) The electronic structure and bonding of an hydrogen pair near a FCC Fe stacking fault. . *Int. J. Hydrogen Energy*. **27**(3) 333-338.

[18] Du, Y. A., Ismer, L., Rogal, J., Hickel, T., Neugebauer, J. and Drautz, R. (2011) First-principles study on the interaction of H interstitials with grain boundaries in α- and γ-Fe. *Phys. Rev. B*. **84**(14) 144121(1)-144121(13).

[19] Jiang, D. E. and Carter, E. A. (2003) Adsorption and diffusion energetics of hydrogen atoms on Fe(110) from first principles. *Surf. Sci.* **547**(1) 85-98.

[20] Jiang, D. E. and Carter, E. A. (2004) Diffusion of interstitial hydrogen into and through bcc Fe from first principles. *Phys. Rev. B*. **70**(6) 064102(1)-064102(9).

[21] Sholl, D. S. (2007) Using density functional theory to study hydrogen diffusion in metals: A brief overview. *J. Alloys Compd.* **446** 462-468.

[22] Grabke, H. J. and Riecke, E. (2000) Absorption and diffusion of hydrogen in steels. *Mater. Tehnol.* **34**(6) 331-342.

[23] Kresse, G. and Furthmüller, J. (1996) Efficiency of ab-initio total energy calculations for metals and semiconductors using a plane-wave basis set. *Comp. Mater. Sci.* **6**(1) 15-50.

[24] Perdew, J. P., Burke, K. and Ernzerhof, M. (1996) Generalized Gradient Approximation Made Simple. *Phys. Rev. Lett.* **77**(18) 3865-3868.

[25] Blöchl, P. E. (1994) Projector augmented-wave method. *Phys. Rev. B*. **50**(24) 17953-17979.

[26] Ismer, L., Hickel, T. and Neugebauer, J. (2010) Ab initio study of the solubility and kinetics of hydrogen in austenitic high Mn steels. *Phys. Rev. B*. **81**(9) 094111(1)- 094111(9).

[27] Medvedeva, N. I., Van Aken, D. and Medvedeva, J. E. (2010) Magnetism in bcc and fcc Fe with carbon and manganese. *J. Phys. Condens. Matter*. **22**(31) 316002(1)-316002(7).

[28] Jiang, D. E. and Carter, E. A. (2003) Carbon dissolution and diffusion in ferrite and austenite from first principles. *Phys. Rev. B*. **67**(21) 214103(1)-214103(11).

[29] Herper, H. C., Hoffmann, E. and Entel, P. (1999) Ab initio full-potential study of the structural and magnetic phase stability of iron. *Phys. Rev. B*. **60**(6) 3839-3848.

[30] Dyson, D. J. and Holmes, B. (1970) Effect of alloying additions on the lattice parameter of austenite. *J. Iron Steel Inst.* **208**(5) 469-474.

[31] Methfessel, M. P. A. T. and Paxton, A. T. (1989) High-precision sampling for Brillouin-zone integration in metals. *Phys. Rev. B*. **40**(6) 3616-3621.

[32] Payne, M. C., Teter, M. P., Allan, D. C., Arias, T. A. and Joannopoulos, J. D. (1992) Iterative minimization techniques for ab initio total-energy calculations: molecular dynamics and conjugate gradients. *Rev. Mod. Phys.* **64**(4) 1070-1072.

[33] Pack, J. D. and Monkhorst, H. J. (1976) Special points for Brillouin-zone integrations. *Phys. Rev. B: Condens. Matter*. **13**(12) 5188-5192.

[34] Bacher, J. P., Benvenuti, C., Chiggiato, P., Reinert, M. P., Sgobba, S. and Brass, A. M. (2003) Thermal desorption study of selected austenitic stainless steels. *J. Vac. Sci. Technol*. **21**(1) 167-174.

[35] Bernstein, I. M. (1970) The role of hydrogen in the embrittlement of iron and steel. *Mater. Sci. Eng. R-Rep*. **6**(1) 1-19.

[36] Brass, A. M. and Chêne, J. (2006) Hydrogen uptake in 316L stainless steel: Consequences on the tensile properties. *Corros. Sci.* **48**(10) 3222-3242.

[37] Chen, Y., Santos, D. M. and Sequeira, C. A. (2006) Hydrogen Diffusion in Austenitic Stainless Steels. *Trans. Tech. Publ.* **258** 322-326.

[38] Deng, B. Q., Huang, Q. R., Peng, L. L., Mao, O., Du, J. J., Lu, Z. and Liu, X. Z. (1992) Measurement of hydrogen solubility, diffusivity and permeability in HR-1 stainless steel. *J. Nucl. Mater.* **191** 653-656.

[39] Grant, D. M., Cummings, D. L. and Blackburn, D. A. (1988) Hydrogen in 316 steel—diffusion, permeation and surface reaction. *J. Nucl. Mater.* . **152**(2-3) 139-145.

[40] Kanezaki, T., Narazaki, C., Mine, Y., Matsuoka, S. and Murakami, Y. (2008) Effects of hydrogen on fatigue crack growth behavior of austenitic stainless steels. *Int. J. Hydrogen Energy*. **33**(10) 2604-2619.

[41] Louthan, M. R. and Derrick, R. G. (1975) Hydrogen transport in austenitic stainless steel. *Corros. Sci.* **15**(6-12) 565-577.

[42] Zielinski, A. (1990) Effect of hydrogen on internal friction of some FCC metals. *Acta Mater.* **38**(12) 2573-2582.

Figures

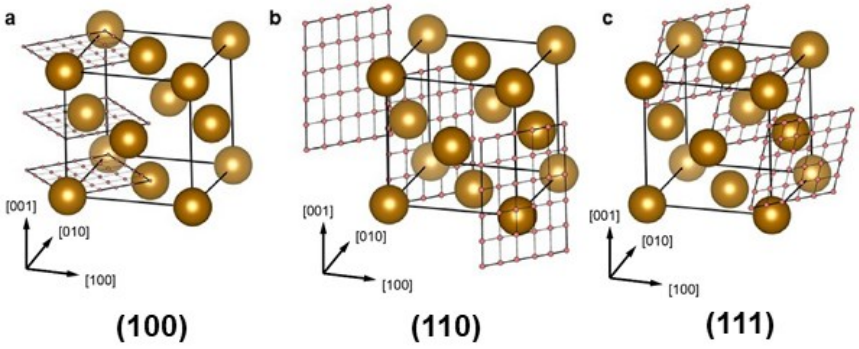

Figure 1: The calculation mesh for the (a) (100), (b) (110), and (c) (111) surfaces. Only three of the nine calculation meshes are displayed for each surface for clarity.

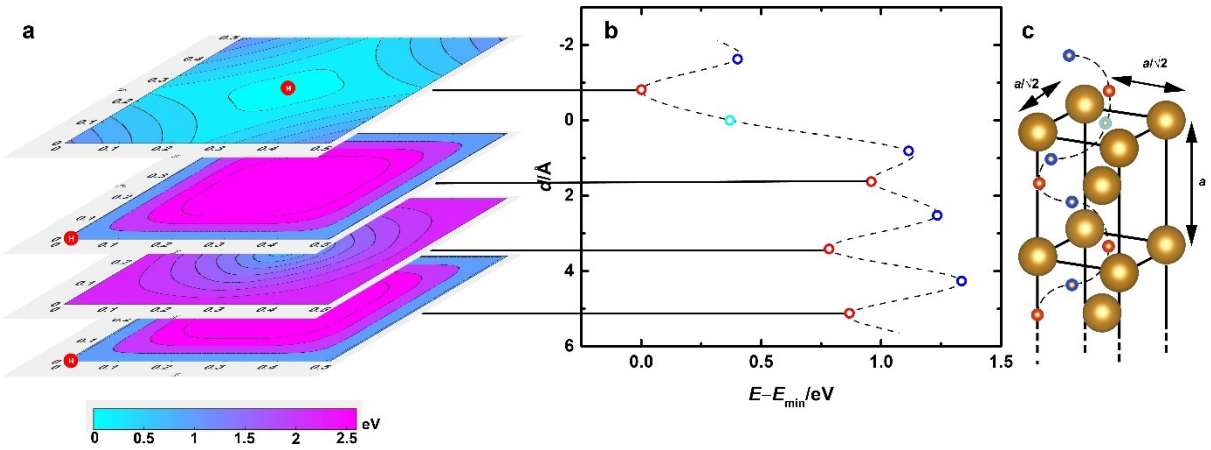

Figure 2: (a) The 2D potential energy surface at local minima for hydrogen diffusion through the (100) surface. (b) The energy profile for hydrogen diffusion through the surface. (c) The diffusion pathway from the surface through towards the bulk. The dotted line between stationary points is only a guide to the eye.

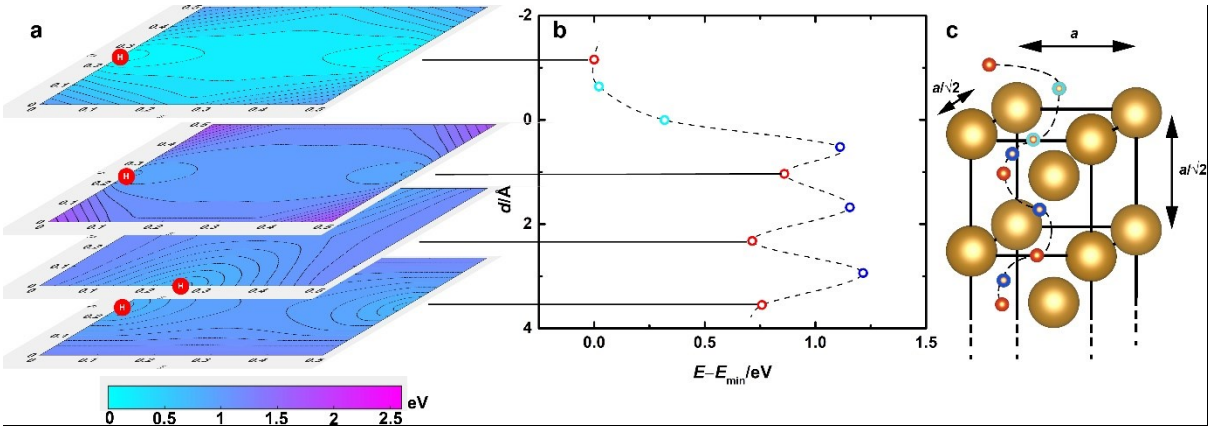

Figure 3: (a) The 2D potential energy surface at local minima for hydrogen diffusion through the (110) surface. (b) The energy profile for hydrogen diffusion through the surface. (c) The diffusion pathway from the surface through towards the bulk. The dotted line between stationary points is only a guide to the eye.

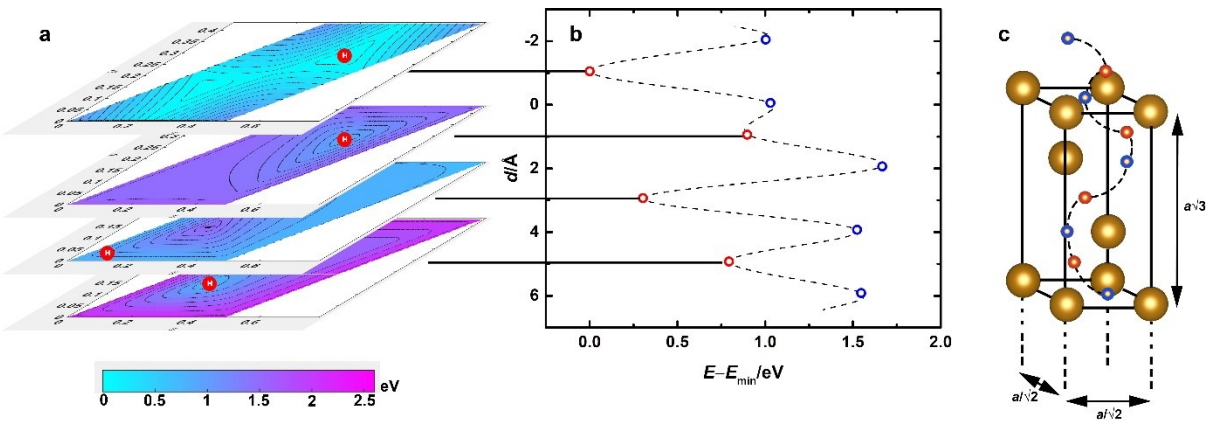

Figure 4: (a) The 2D potential energy surface at local minima for hydrogen diffusion through the (111) surface. (b) The energy profile for hydrogen diffusion through the surface. (c) The diffusion pathway from the surface through towards the bulk. The dotted line between stationary points is only a guide to the eye.

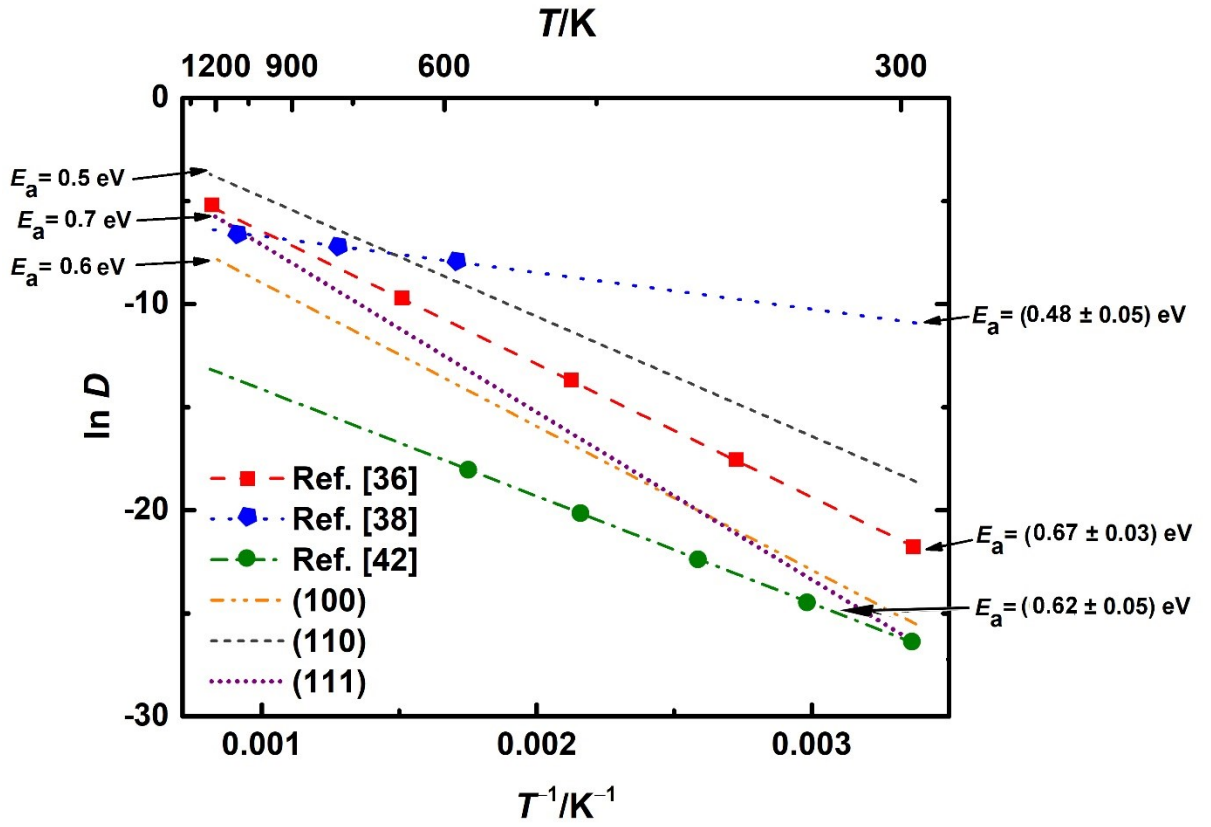

Figure 5: Arrhenius plot of the diffusion coefficients as a function of temperature, comparing experimental literature data with our calculations for the (100), (110) and (111) surfaces. The activation energy, E_a is labelled for each dataset. The graphs are offset for clarity.

Tables

Table 1: Relative minimum energies, E-E_{min}, for H in each layer, i, considered in this work for all three surfaces; see also Fig. 2, 3, and 4. Each energy is calculated relative to the minimum energy for a particular surface. Brackets behind the zero values in the table indicate the preferential adsorption site on the surface.

Layer index, *i*	**Surface index**		
	(100)	**(110)**	**(111)**
	E-E_{min}/eV		
1	0.40	0.00 (sb)	1.00
2	0.00 (4f)	0.02	0.00 (3f)
3	0.37	0.32	1.0
4	1.12	1.11	0.90
5	0.96	0.86	1.67
6	1.23	1.16	0.30
7	0.78	0.71	1.52
8	1.34	1.22	0.79
9	0.87	0.76	1.55